J Mar Sci Technol (2007) 12:1–14
DOI 10.1007/s00773-006-0232-7

ORIGINAL ARTICLE

Prediction method of hydrodynamic forces acting on the hull of a blunt-body ship in the even keel condition

Donghoon Kang · Kazuhiko Hasegawa

Received: January 3, 2006 / Accepted: August 4, 2006

Abstract The mathematical modeling group (MMG) model is well known and is widely used in the field of ship maneuverability. However, the MMG model can be applied only after determination of the hydrodynamic coefficients either from comprehensive captive model tests or from general empirical data. Around the cruising speed, when a ship's drift angle is relatively small, several methods have been developed to predict hydrodynamic coefficients from the ship's principal particulars, e.g., Kijima's method. Kijima's method is efficient in predicting the ship's maneuverability at the initial design stage and is even able to assess the effect of changes in stern design. Similarly, for the low speed range when a ship's drift angle is relatively large, several methods for predicting the ship's hydrodynamic coefficients have been proposed, based on captive model tests, such as those by Kose, Kobayashi, and Yumuro. However, most of the methods developed for low speeds cannot be applied to general ship types without additional experiments being performed. In contrast, Karasuno's method uses theoretical and empirical approaches to predict the hydrodynamic forces, even for large drift motions. Although Karasuno's model utilizes the ship's principal particulars and is applicable to a general vessel, it has not been widely used. This is because the form of Karasuno's model is relatively complicated and its accuracy around the cruising speed is less than that for other methods that have been specifically developed for the cruising speed range. A practical method for predicting hydrodynamic forces for the entire operating speed range of blunt-body ships is proposed in this article. It is based on the MMG model and predicts hydrodynamic coefficients based on a ship's principal particulars. A regression model for the proposed method has also been proposed by analyzing 21 different blunt-body ships. Finally, simulations of a very large 4-m crude carrier (VLCC) model using the proposed method were carried out and the results compared with free-running experiments (both at the cruising speed and at low speeds) to validate the efficacy of the model.

Key words Hydrodynamic force · Low speed · Highly oblique motion · MMG model

D.H. Kang (✉) · K. Hasegawa
Department of Naval Architecture and Ocean Engineering, Graduate School of Engineering, Osaka University, 2-1 Yamadaoka, Suita 565-0871, Japan
e-mail: Kang_Dong_Hoon@naoe.eng.osaka-u.ac.jp

List of symbols

a_H	ratio of hydrodynamic force induced on ship hull by rudder action to the rudder force
ax2, ax4, bx1, bx2	hydrodynamic coefficients of the surge force
ay1, ay3, ay5, cy1, dy1, ey1	hydrodynamic coefficients of the sway force
an2, an4, cn2, dn0, dn2, en0	hydrodynamic coefficients of the yaw moment
A_R	rudder area
B	ship breadth
C_b	block coefficient
C_{pa}	prismatic coefficient of the aft hull
C_{RS}, C_{RP}	coefficients of inflow velocity for the starboard and port rudder, respectively
C_{wa}	water plane area coefficient of the aft hull

d	ship draft
D_P	propeller diameter
e_a	stern hull form parameter (1) defined by Mori[14]
e'_a	stern hull form parameter (2) defined by Mori
K	stern hull form parameter (3) defined by Mori
σ_a	stern hull form parameter (4) defined by Mori
F_{NS}, F_{NP}	rudder normal force for the starboard and port rudder, respectively
h_R	rudder height
I_{zz}	yaw moment of inertia
J_s	advance ratio
J_{zz}	added yaw moment of inertia
k	ship aspect ratio
L	ship length
m	ship mass
m_x	added mass in surge
m_y	added mass in sway
$N_H, N_R, N_A = (1/2\rho L^2 dU^2)\cdot(N'_H), (N'_R), (N'_A)$	yaw moment components of hull, rudder, and wind acting on the ship
n	propeller revolutions
P	propeller pitch
$r = r'\cdot(U/L)$	yaw rate at ship's center
rps	propeller revolutions
$R'(u)$	nondimensional ship resistance
S_W	wetted surface area
t_R	coefficient for additional drag of the rudder
u	surge velocity
U	ship velocity
v	sway velocity
x_G	longitudinal center of gravity of the ship
x_H	ratio of hydrodynamic moment induced on the ship hull by rudder action to the rudder force
x_R	x-coordinate of the rudder location
x_t	longitudinal center of gravity of added mass of the ship
$X_H, X_P, X_R, X_A = (1/2\rho LdU^2)\cdot(X'_H), (X'_P), (X'_R), (X'_A)$	x-axis components of hull, propeller, rudder, and wind force acting on the ship
X_M	measured force in the x-axis direction during the captive model test
X_{vr}	hydrodynamic coefficient for surge force from Hasegawa's chart
$Y_H, Y_R, Y_A = (1/2\rho LdU^2)\cdot(Y'_H), (Y'_R), (Y'_A)$	y-axis components of hull, rudder, and wind force acting on the ship
α_{RS}, α_{RP}	starboard and port effective rudder inflow angle
β	drift angle
δ_S, δ_P	starboard and port rudder angles
ε	wake ratio between propeller and rudder
ρ	water density
γ_R	flow straightening factor
ω_P	effective wake fraction
ψ_w	angle of wind encounter

Introduction

Most vessels are tested for their maneuverability during sea trials before delivery; however, maneuvering trials are usually few and are carried out only to check conformance with International Maritime Organization (IMO) standards.[1] It is difficult to use full-scale trials for assessing the maneuverability of a vessel in detail, because they are very expensive and time consuming. Model tests are usually carried out instead of full-scale trials, but they are also relatively expensive and time consuming. In recent years, the need for assessing the maneuverability of vessels has gradually increased for meeting the requirements of design, operation, and simulator facility. In response to this requirement, prediction methods for assessing the maneuverability of vessels have been developed. The IMO has also developed standards for assessing maneuvering performance criteria of vessels using numerical methods at the design stage. From a practical point of view, Kijima[2] and Lee[3] have proposed regression models for assessing hydrodynamic forces acting on the hull (hereinafter, hull forces) using a database of model ship tests. These regression models were developed based on the mathematical modeling group (MMG) model,[4] and are easy to adopt at the design stage. This is because these models are able to predict hull forces using a ship's principal particulars. Kijima's regression model is additionally able to assess the effect of changes in the stern shape, and this model's efficacy at the design stage has been verified. Similarly, Lee's regression model predicts hull forces using parameters of the stern hull form, and it also utilizes propeller particulars as a parameter of the regression model. However, the above-mentioned IMO standards and regression models are only concerned with behavior at the cruising speed.

When a vessel departs from or arrives in a port, it undergoes various complicated maneuvering operations, e.g., course alteration, acceleration, and deceleration. These maneuvering operations are not performed in any particular order; they are performed either individually or in conjunction with one another at various speeds. Although the duration of low-speed operations is short compared to cruising-speed conditions, they are crucial to the safe operation of a ship. This is because low-speed maneuvers are usually performed in restricted areas and are vulnerable to external forces, such as currents, wind, and waves. Despite this fact, low-speed maneuvers are not the central concern for design and research of most ships. Therefore, a need to extend performance assessment to low-speed operations has evolved from simulations and real experience.[5] Several methods have been developed for predicting ship motion at low speeds, such as those of Kose,[6] Kobayashi,[7] Yumuro,[8] and Karasuno.[9] Kose, Kobayashi, and Yumuro's methods were developed for a specific ship having captive model test results, and their results match well with those of the experiments. However, none of the above methods is yet established for a general ship type. Karasuno has proposed a component-type mathematical model for predicting hull forces. Karasuno's model is developed theoretically and empirically using a simplified vortex model and is able to express highly oblique motion of a ship. Karasuno's model can also predict hull forces using a ship's principal particulars, as the Kijima model does; however, it cannot assess the effect of changes in the stern design.

In this article, a practical prediction method for hull forces from the cruising speed to low-speed maneuvers for a blunt-body ship is proposed. The prediction method was developed based on the MMG model to increase its adaptability for a general vessel type. When selecting the equations for the hull forces, the ability to accurately estimate hull forces from the cruising speed to low speeds was the principal focus of this research. For operations around the cruising speed, the results of Kijima's model are used to generate the hydrodynamic forces and moments for the proposed model, while the results of Karasuno's model are used to generate the hydrodynamic forces and moments for the low-speed range where relatively large drift motions are experienced. The proposed method is distinct from Lee's model in the sense that the propeller details need not be fixed for the analysis.

A regression model is proposed for easy application of the proposed method. The regression model has been designed so that the hydrodynamic coefficients can be predicted by using a ship's design parameters only. Twenty-one different blunt-body ships were analyzed with the proposed method to build the regression model. Finally, a very large 4-m crude carrier (VLCC) model was simulated with the proposed method and regression model, and the results of the simulations were compared with the equivalent free-running experiments.

Range of consideration

The characteristics of a maneuvering ship can be expressed in terms of its nondimensional yaw rate (hereinafter r') and drift angle (hereinafter β). To analyze a ship's performance, including that at low speed, the range of consideration of r' and β should first be determined. If an unrealistic operating range is considered, then the accuracy of the predicted hydrodynamic hull forces will be reduced.

It is well known that a ship maneuvering at its cruising speed performs with small r' and β values compared with the values for low-speed maneuvering. Free-running experiments of berthing were carried out to recognize the characteristics of a ship maneuvering at low speed. Table 1 shows the principal particulars of the ship that was used in the experiment. The experiment was conducted as per Endo's berthing procedure.[10] However, during the experiments, the model ship was initially decelerated from half speed to slow speed and only one course alteration was considered; the above procedure was followed because of the restricted nature of the experimental area.

Figure 1 shows the trajectory of the model ship and the time histories of the parameters. From the time histories of v and r it can be concluded that the ship smoothly berthed without being disturbed by external factors such as wind. It may be noted that the increments in v and r after 190 s were caused by the propeller reversing effect. The characteristics of this experiment is shown in Fig. 2 using r' and β. Figure 2 shows the duration of each combination of r' and β as a percentage of the total duration of the experiment. The ship's performance is mainly in the region of small r' and β; the maximum values of r' and β were 1.6 and 90°, respectively. It is noted that the ship's performance is mostly distributed in the first quadrant; this is because the ship performed

Table 1. Principal dimensions of the model ship

L	4.00 m	X_G	0.123 m
B	0.667 m	S_W	4.049 m^2
d	0.240 m	D_P	0.12057 m
C_b	0.817	P / D_P	0.6669

The rudder was a mariner type super VecTwin

Fig. 1. Trajectory and time histories of parameters for the berthing experiment

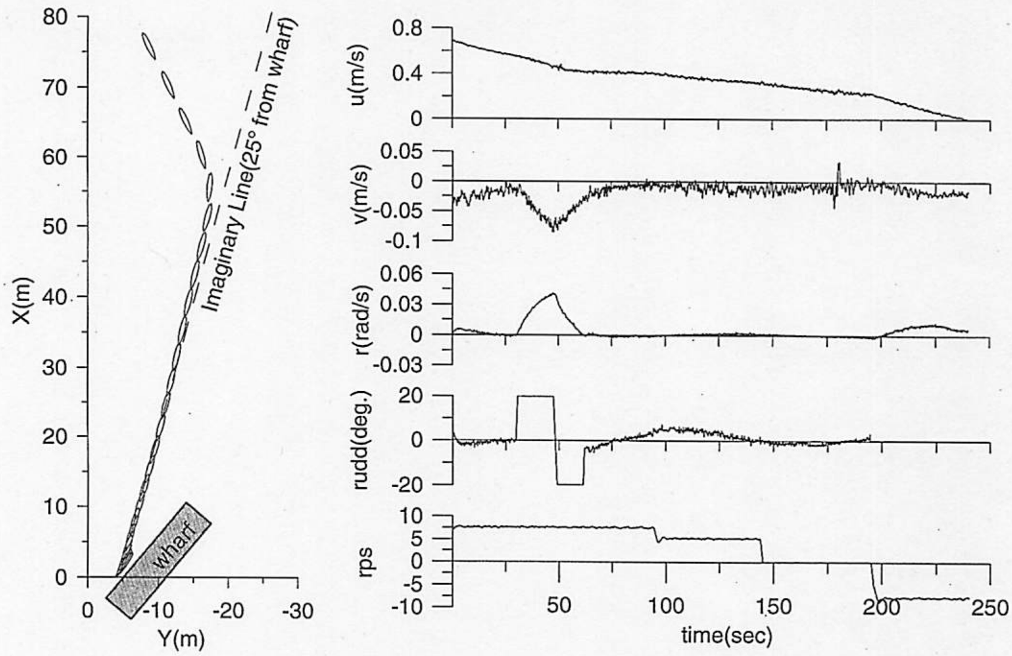

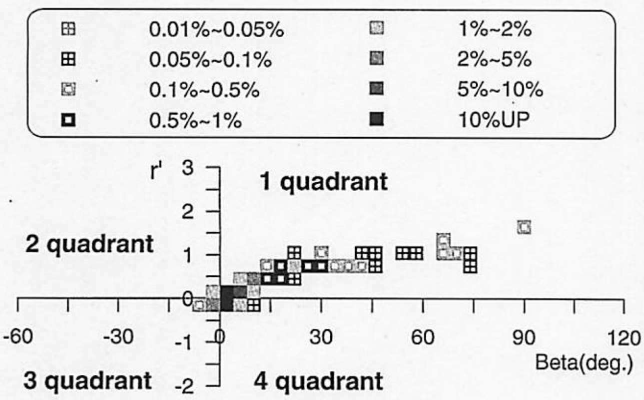

Fig. 2. Characteristics of ship performance for the berthing experiment. The percentages indicate the duration of each combination of r' and β compared to the total duration of the experiment

a starboard course alteration only and was operated with a counterclockwise-rotating propeller for stopping. If the ship's operating conditions were reversed, i.e., turning to port and using a clockwise-rotating propeller for stopping (e.g., controllable pitch propeller), then the ship's performance would move to the third quadrant.

Figure 3 shows the time histories for two different experiments for the time from the propeller stop to the propeller astern condition; this is one of the most extreme cases of low-speed maneuvering. Case 1 is part of the experiment shown in Fig. 1 and case 2 is an example of when the ship is affected by wind. The influence of the wind can easily be recognized when the sway velocity and the yaw rate increase before the propeller is reversed in case 2. The characteristics of these two experiments

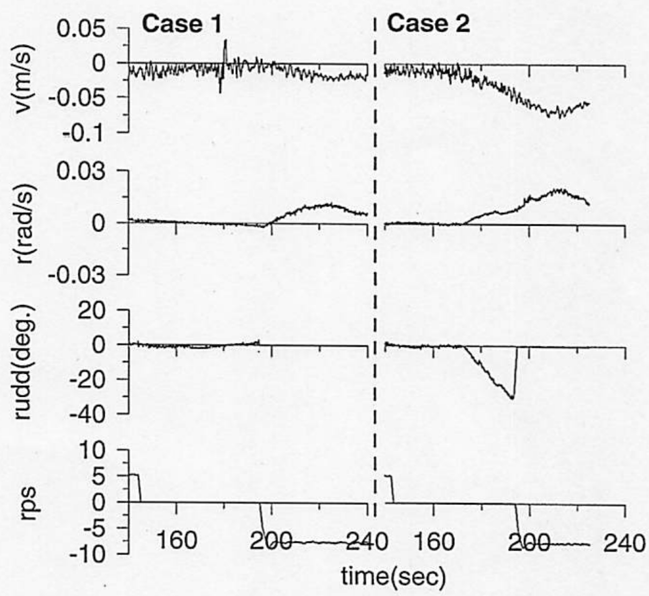

Fig. 3. Time histories of two different berthing experiments from the time of propeller stop. Case 1, the data from Fig. 2; case 2, the ship is affected by wind

are shown in Fig. 4; the method of analysis was same as that followed in Fig. 2. In case 2, the relative duration of large β is increased compared to that of case 1, but the maximum r' value is decreased. This is because the sway velocity was increased by the wind and the total ship velocity was thereby increased. Even the yaw rate was increased by the wind, although r' is not increased significantly because of the increase in total ship velocity.

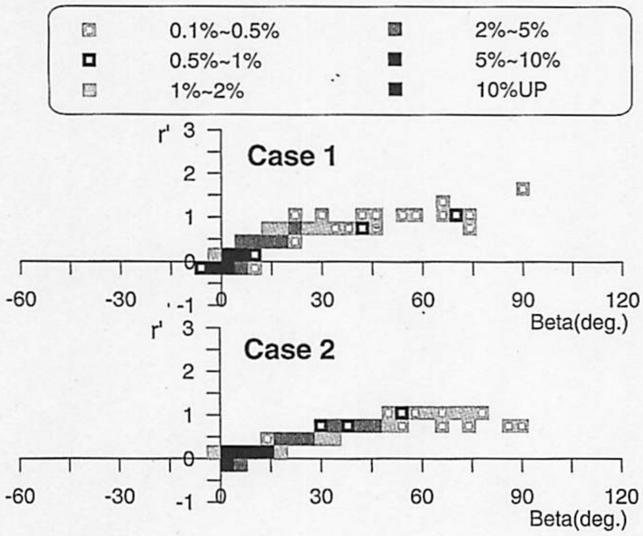

Fig. 4. Characteristics of ship performance for berthing experiments from the time of propeller stop

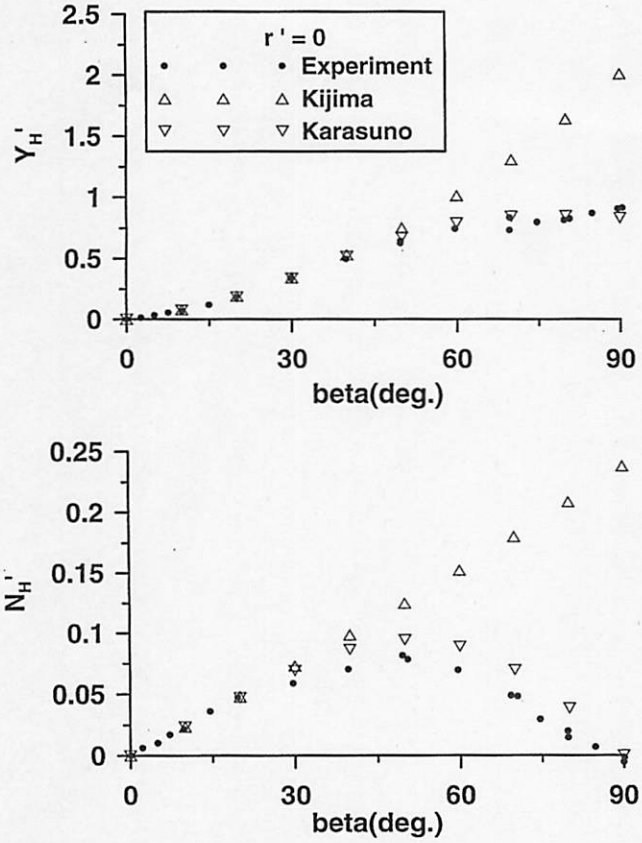

Fig. 5. Experimental and calculated values of Y'_H and N'_H at $r' = 0$

Considering the above results, the ranges of r' and β to be considered in the current work were set as ($0 \le r' \le 1.6$, $0° \le \beta \le 90°$) and ($-1.6 \le r' \le 0$, $-90° \le \beta \le 0°$) respectively. In astern motion, relatively large values of r' and β occur in the second and fourth quadrants; because the astern condition was not researched in this work, the corresponding range of r' and β were ignored.

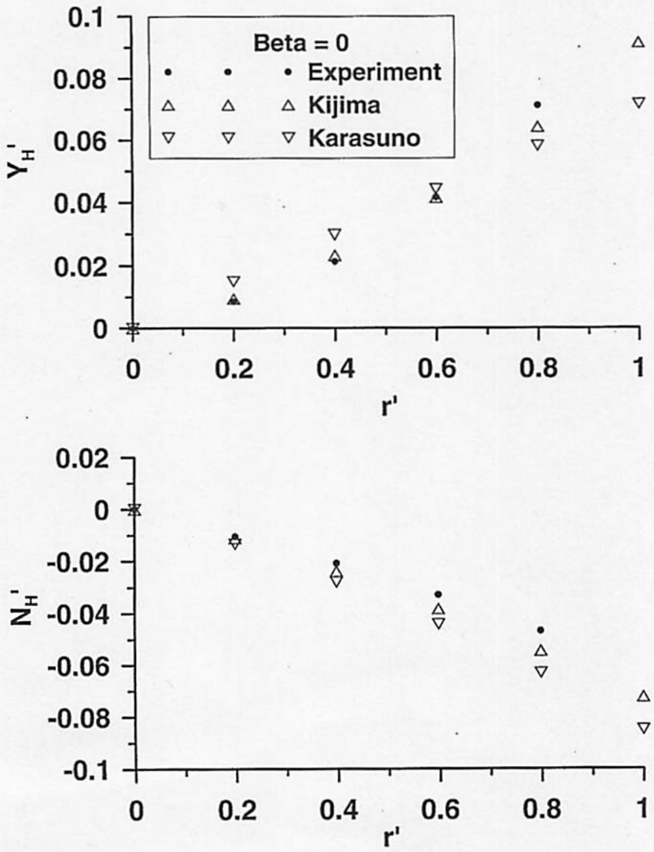

Fig. 6. Experimental and calculated values of Y'_H and N'_H at $\beta = 0$

Base calculation of hull forces

In this research, the hull forces calculated by Kijima's method and Karasuno's method are used as a reference, but the range over which these methods give accurate results must first be determined. The hull forces of the VLCC *Esso Osaka* were calculated using Kijima's and Karasuno's methods and compared with experimental results.[8] Figures 5 and 6 show the results of experiments and those of Kijima's and Karasuno's methods for Y'_H and N'_H for the *Esso Osaka* under different conditions. The conditions for the calculations and experiments are $r' = 0$ for Fig. 5 and $\beta = 0$ for Fig. 6.

From Fig. 5, it can be observed that Karasuno's method well represents the trend of experimental results up to $\beta = 90°$. As expected, the results using Kijima's method have a marked deviation from the experimental data for $\beta > 20°$. From Fig. 6 it can be observed that Kijima's method accurately represents experiment results for small β. Generally, Kijima's method matches well with the experimental results below drift angles of 20°, while Karasuno's method well describes the trend of the overall experimental data.

Considering the accuracy and continuity of Kijima's and Karasuno's methods, Kijima's method was used up to $\beta = 30°$, while Karasuno's method was used for the rest of range to calculate the hull forces of a ship. These are considered as base data for this research. It is noted that the experimental data for X'_H for the *Esso Osaka* have not been published, so the comparison for X'_H has been omitted here. It is well known that X_{vr} from Hasegawa's chart[11] well expresses X'_H for small β values; Kijima's method also uses X_{vr} for expressing X'_H. In the current work, the base data for X'_H was generated by using X_{vr} up to $\beta = 30°$, while for $\beta > 30°$ the base data for X'_H was generated by using Karasuno's method.

Equations of ship maneuvering

The equations of a maneuvering ship were written as per the MMG model. The mathematical model of ship maneuvering motion was described based on three degrees of freedom: surge, sway, and yaw. The equations of ship maneuvering motion are written as:

$$\begin{aligned}
&(m+m_x)\cdot\dot{u} - m\cdot(v\cdot r + x_G\cdot r^2) = X \\
&(m+m_y)\cdot\dot{v} + (m\cdot x_G + m_y\cdot x_t)\cdot\dot{r} + m\cdot u\cdot r = Y \\
&(I_{zz} + m\cdot x_G^2 + J_{zz} + m_y\cdot x_t^2)\cdot\dot{r} + (m\cdot x_G + m_y\cdot x_t)\cdot\dot{v} \\
&\quad + m\cdot x_G\cdot u\cdot r = N
\end{aligned} \tag{1}$$

The external forces X, Y, and moment N consist of hull, rudder, and wind components as follows:

$$\begin{aligned}
X &= X_H + X_P + X_R + X_A \\
Y &= Y_H + Y_R + Y_A \\
N &= N_H + N_R + N_A
\end{aligned} \tag{2}$$

Figure 7 shows the coordinate system and the definition of various parameters.

Expression of hull forces

To develop and select the equations for expressing the hull forces as mentioned above, the ability to accurately and continuously estimate the hull forces for the entire range of ship speeds is regarded as important. The physical meanings of terms that are components of the equations were not considered important. Equations 3–5 are used for expressing the hull forces of a ship. Equation 3, for the surge force, was developed by estimating the surge force for a wide rage of r' and β values. Equations 4 and 5 for the sway force and yaw moment were taken from Yumuro's proposal:[8]

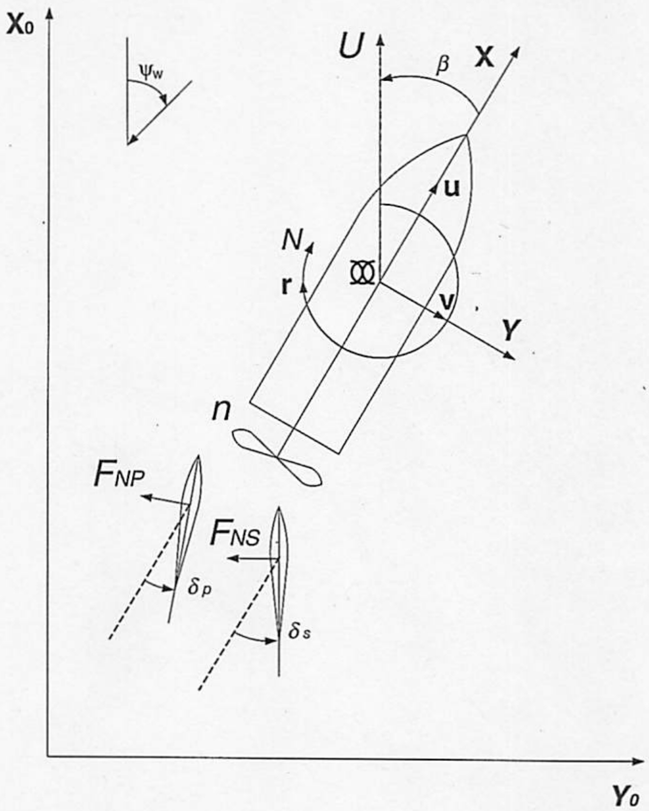

Fig. 7. Coordinate system

$$\begin{aligned}
X'_H &= (\mathrm{ax2}\cdot\sin^2(\beta) + \mathrm{ax4}\cdot\sin^2(2\beta))\cdot\cos(\beta) \\
&\quad + \mathrm{bx1}\cdot\sin(\beta)\cdot r' \\
&\quad + \mathrm{bx2}\cdot\sin(2\beta)\cdot r'\cdot\mathrm{sign}(\cos(\beta)) + R'(u)
\end{aligned} \tag{3}$$

$$\begin{aligned}
Y'_H &= (\mathrm{ay1} + \mathrm{cy1}\cdot r'^2)\cdot\sin(\beta) \\
&\quad + \mathrm{ay3}\cdot\sin(3\beta) + \mathrm{ay5}\cdot\sin(5\beta) \\
&\quad + (\mathrm{dy1}\cdot r' + \mathrm{ey1}\cdot r'^3)\cdot\cos(\beta)
\end{aligned} \tag{4}$$

$$\begin{aligned}
N'_H &= (\mathrm{an2} + \mathrm{cn2}\cdot r'^2)\cdot\sin(2\beta) \\
&\quad + \mathrm{an4}\cdot\sin(4\beta) + \mathrm{dn0}\cdot r' \\
&\quad + \mathrm{en0}\cdot r'^3 + \mathrm{dn2}\cdot r'\cdot\cos(2\beta)
\end{aligned} \tag{5}$$

The results obtained from Kijima's and Karasuno's methods are used as the base data, as mentioned earlier. The base data were posited as the results of experiments and analyzed as per the method of analyzing experimental data[12,13] to generate hydrodynamic coefficients such as ax2 and dn2 in Eqs. 3–5. The analysis to determine whether the developed and selected equations well express the base data was carried out for the *Esso*

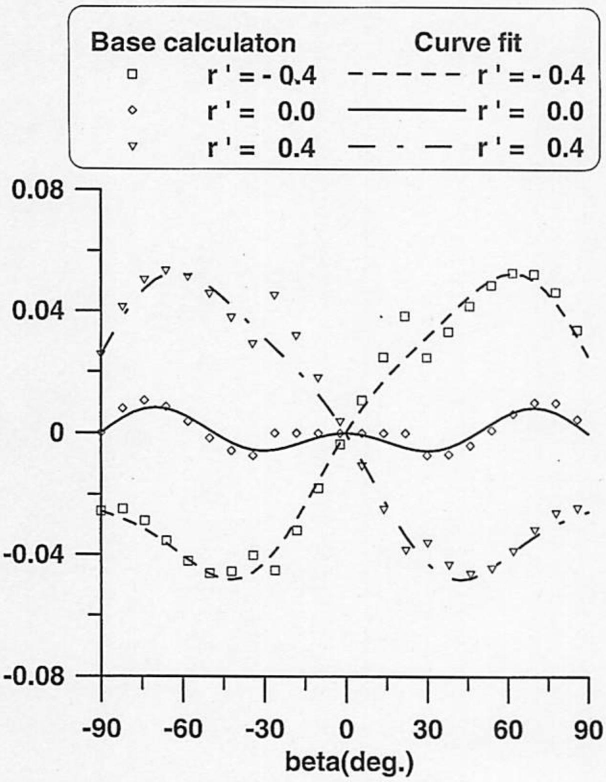

Fig. 8. Base data and calculations for X'_H

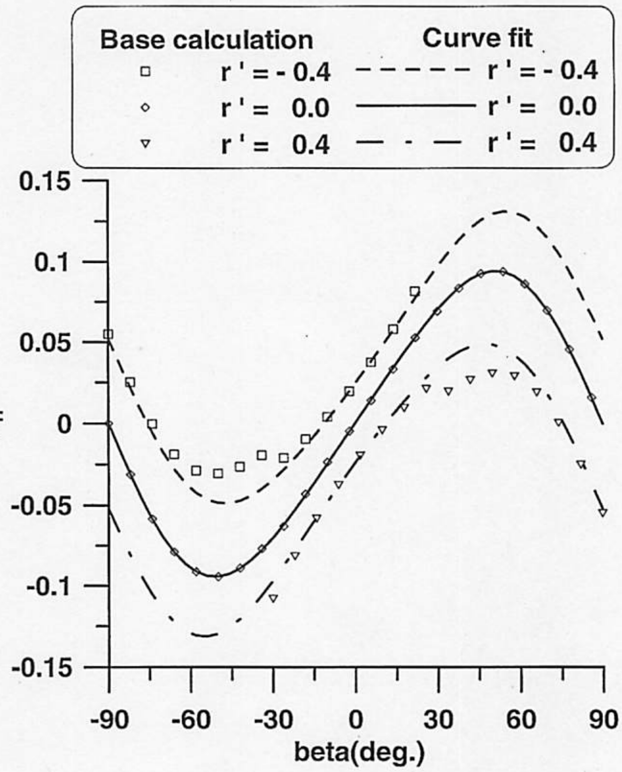

Fig. 10. Base data and calculations for N'_H

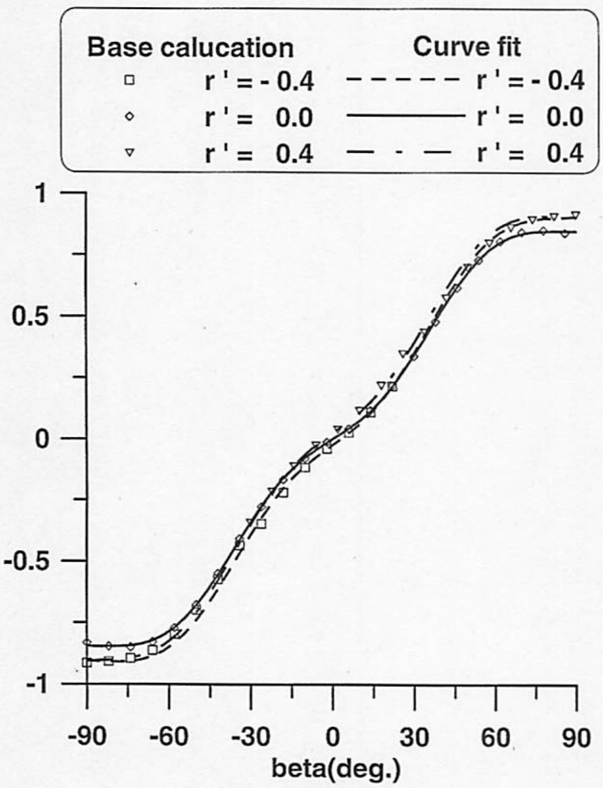

Fig. 9. Base data and calculations for Y'_H

Osaka. The hydrodynamic coefficients in Eqs. 3–5 were determined by the above-mentioned analysis method. Hull forces and moments for the *Esso Osaka* were calculated again using the determined coefficients for $-90° \leq \beta \leq 90°$ so as to validate the equations; the results are shown in Figs. 8–10. It can be observed that Eqs. 3–5 match well with the base data for the range $-90° \leq \beta \leq 90°$ and $-1.6 \leq r' \leq 1.6$. This range of parameters was earlier shown to define the domain of low-speed as well as cruising-speed maneuvering. Equations 3–5 can be used for simulating berthing maneuvers in which the ship decelerates from cruising speed to low speed, which until now has been difficult with other models, as described earlier. It may also be noted that although the equations are designed for $|\beta| \leq 90°$, they are also able to express the tendency of the hull forces for $|\beta| \geq 90°$.

Regression model for a blunt-body ship

A regression model for a blunt-body ship at even keel is here proposed for easy application of the above method. The hull forces and moments were calculated for 21 different blunt-body ships using the proposed method, and the hydrodynamic coefficients for each ship were

Table 2. List of dimensions of blunt-body ships used to develop the regression model

	L (m)	B (m)	d (m)	C_b
Ship-A	4.5000	0.7430	0.2800	0.8330
Ship-B	4.4000	0.7932	0.2834	0.8310
Ship-C	3.0000	0.4893	0.2011	0.8310
Ship-D	6.0000	0.9785	0.4012	0.8290
Ship-E	4.0000	0.8000	0.2930	0.8200
Ship-F	3.8280	0.6344	0.2111	0.8197
Ship-G	4.0000	0.6667	0.2400	0.8170
Ship-H	4.0000	0.7270	0.2600	0.8100
Ship-I	4.0000	0.7270	0.2600	0.8090
Ship-J	4.0000	0.7270	0.2600	0.8090
Ship-K	3.5000	0.7000	0.2111	0.8048
Ship-L	3.5000	0.6344	0.2111	0.8045
Ship-M	3.5000	0.6344	0.2111	0.8033
Ship-N	6.0000	0.9994	0.3619	0.8027
Ship-O	6.0000	0.9994	0.3619	0.8021
Ship-P	3.5000	0.7000	0.2111	0.8019
Ship-Q	3.5000	0.6344	0.2111	0.8018
Ship-R	6.0000	0.9994	0.3619	0.8017
Ship-S	5.0000	0.8333	0.3000	0.7926
Ship-T	3.1719	0.6344	0.2111	0.7834
Ship-U	3.0000	0.4962	0.2008	0.7770

Ship-I and Ship-J have different stern hull forms

Table 3. Parameters for the regression model

Ship parameter	Stern hull form parameter
L	$e_a=\frac{L}{B}\cdot(1-C_{pa})$
B	$e_a'=\frac{e_a}{\sqrt{\frac{1}{4}+\frac{1}{(B/d)^2}}}$
d	
C_b	$\sigma_a=\frac{1-C_{wa}}{1-C_{pa}}$
$k=2\cdot\frac{d}{L}$	$K=\left(\frac{1}{e_a'}+\frac{1.5}{L/B}-0.33\right)\cdot(0.95\sigma_a+0.40)$

determined using Eqs. 3–5. The principal particulars of these 21 ships are shown in Table 2. After determining the hydrodynamic coefficients, the regression model for each coefficient was developed. The parameters for the regression model were set as shown in Table 3. It may be noted that this model also utilizes parameters for the stern hull form,[14] so it is able to express hull forces corresponding to changes in the stern hull form, as for Kijima's model.

More than 300 combinations of parameters were tested for each coefficient, and suitable equations for predicting each coefficient were determined. The maximum average percentage error (A.P.E.), as defined by Eq. 6, was 10.66. Figure 11 is an example that shows ax2 with an A.P.E. of 5.19. It should be noted that A.P.E. is not the accuracy index of this regression model for a real

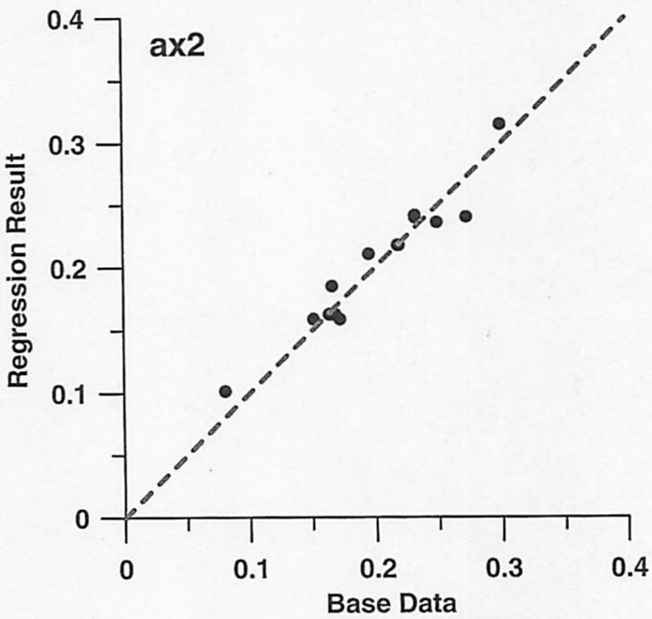

Fig. 11. Base data and regression results for parameter ax2

ship, because the base data themselves were the predicted values using Kijima's and Karasuno's methods.

$$A.P.E=\left|(y_i-y_p)/y_i\right|\times 100/n\_ship \tag{6}$$

where, y_i is the original value from the base data, y_p is the predicted value using the regression model, and n_ship is the total number of ships.

The regression model is shown in Eqs. 7–9:

$$\left.\begin{aligned}
ax2&=\frac{B}{L}\cdot\left(-0.54867+11.791\cdot\frac{d}{L}\right)\\
ax4&=k\left(-0.07237-0.52608\cdot\frac{B}{L}\right)\\
bx1&=0.01835-1.2425\cdot\frac{d}{L}\\
bx2&=-0.0333-0.55842\cdot\frac{d}{L}
\end{aligned}\right\} \tag{7}$$

$$\left.\begin{aligned}
ay1&=0.50194+5.3541\cdot\frac{d}{L}\\
ay3&=-0.08788+0.73174\cdot\frac{C_bB}{L}\cdot K\\
ay5&=-0.10285+1.9317\cdot\frac{d(1-C_b)}{B}\cdot K\\
cy1&=k\cdot\left(12.69-131.63\cdot\frac{C_bB}{L}+430.7\cdot\left(\frac{C_bB}{L}\right)^2\right)\\
dy1&=\frac{B}{L}\cdot(-0.53782+6.6751\cdot k)\\
ey1&=-0.09165+0.16968\cdot\frac{C_bd}{B}\cdot e_a'
\end{aligned}\right\} \tag{8}$$

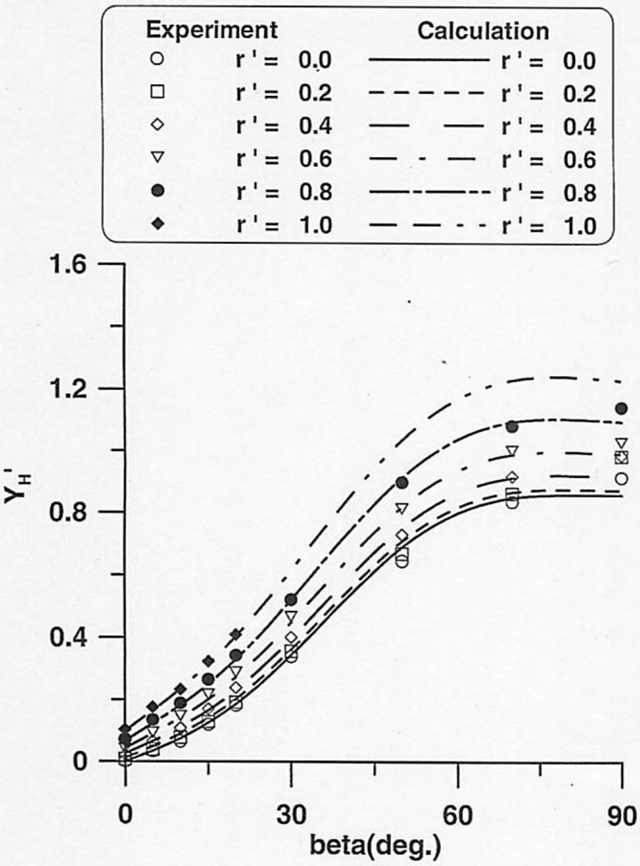

Fig. 12. Experimental data and calculations for Y_H'

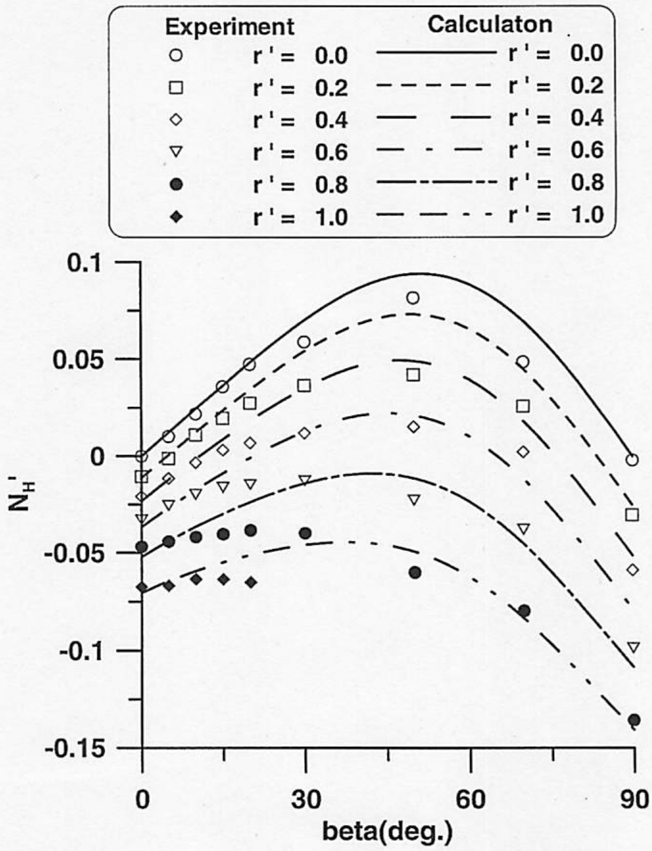

Fig. 13. Experimental data and calculations for N_H'

$$\left.\begin{aligned}
\text{an2} &= \frac{B}{L}\cdot\left(0.07093+1.1936\cdot\frac{d}{B}\right)\\
\text{an4} &= K\cdot\left(-0.052545+0.42428\cdot\frac{C_bB}{L}K\right)\\
\text{cn2} &= \frac{d}{B}\cdot\left(-0.14737+0.43812\cdot\frac{d(1-C_b)}{B}e_a{}'\right)\\
\text{dn0} &= -0.06338-1.253\cdot\frac{d(1-C_b)}{B}\cdot K\\
\text{dn2} &= k\cdot\left(0.46815-0.82503\cdot C_be_a{}'\,k\right)\\
\text{en0} &= -0.04755+0.10488\cdot K
\end{aligned}\right\} \qquad (9)$$

To validate the above equations, the *Esso Osaka* was analyzed with the regression model and the hull forces and moments were compared to the experimental data.[8] Figures 12 and 13 show the results for the sway force and yaw moment. The calculations of the sway force match well with the experimental data. For the yaw moment, the calculation does not match well with the experimental data for 30° < β < 70°. There are two reasons for this. First, the yaw moments predicted by Karasuno's method are slightly larger than those determined by experimental data. Second, the slope of the yaw moment predicted by

Table 4. Applicable parameter ranges of blunt-body ships used for the regression model

Ship parameter	Min	Max
B/L	0.163	0.2
d/L	0.055	0.073
d/B	0.302	0.411
C_b	0.777	0.833

Kijima's method for $\beta \leq 30°$ is such that it tends to increase the yaw moment for $\beta \geq 30°$. The result of these two factors is that the predicted yaw moment is higher. However, the overall tendency of the calculated yaw moment is still reasonable and the calculations match well with the experimental data in the region of small β and $\beta = 90°$. The limits of the design particulars of the 21 different blunt-body ships that were analyzed for developing this regression model are shown in Table 4.

Validation with simulation

Several simulations were also carried out and compared with free-running experiments to validate the proposed method and regression model. A 4-m model VLCC tanker, which was also used for the berthing experiments mentioned earlier, was used for the simulations and the experiment.

It may be observed that the initial conditions for some of the free-running experiments were not ideal. Maximum effort was made to keep the initial conditions of the experiments, such as the sway speed and yaw rate, equal to zero. However, some of the experiments commenced with a small deviation. It may be noted that since the experiments were carried out outdoors, it was difficult to start with the desired initial conditions. Another reason for the deviation is the real-time kinematic global positioning system (RTK-GPS) system that was used for calculating the surge and sway speeds. The RTK-GPS system had an accuracy level of ±0.03 m. The initial conditions for the simulations were set considering the above factors.

Simulation model

For the simulations, the proposed method and regression model were used for calculating the hull forces, while the other forces and moments were taken from Hasegawa.[15] Additional experiments were carried out to increase the accuracy of the mathematical rudder model. The experimental conditions are shown in Table 5.

Hamamoto's expression[16] is used to express the hydrodynamic forces and moment resulting from the VecTwin rudder, and is written as:

$$\left.\begin{aligned} X_R &= -(1-t_R)(F_{NS}\sin\delta_S + F_{NP}\sin\delta_P) \\ Y_R &= -(1+a_H)(F_{NS}\cos\delta_S + F_{NP}\cos\delta_P) \\ N_R &= -(x_R + a_H x_H)(F_{NS}\cos\delta_S + F_{NP}\cos\delta_P) \end{aligned}\right\} \quad (10)$$

The interaction coefficients of the hull and rudder (t_r, a_H, x'_H) were determined from towing tank experiments. Figure 14 shows the interaction between the hull, propeller, and rudder in the surge direction. The gradient of the graph is $1 - t_r$, because the vertical axis is the sum of the rudder forces and the horizontal axis is the rudder forces acting on the hull. The gradient of this graph for each set of experimental data does not vary significantly with the ship's velocity and the propeller revolutions. Therefore, t_r was considered to be a constant value in the simulations. The interaction coefficients between the hull and the rudders in the sway and yaw directions (a_H and x'_H) were similarly analyzed. The coefficients were different as per the experimental conditions. The plot of a_H versus J_S is shown in Fig. 15. The values of a_H were obtained by fitting a second-order polynomial through the experimental data with the additional assumption that $a_H = 0$ when $J_S = 0$. The plot of x'_H versus J_S is shown in Fig. 16. The values of x'_H were obtained by fitting a straight line through the experimental data.

To express the normal forces of the VecTwin rudder, Hasegawa's proposal[15] was used:

Table 5. Experimental conditions for model validation

	Speed (m/s)	rps	J_S
Case 1	0.2	7	0.237
Case 2	0.4	7	0.474
Case 3	0.4	13.7	0.242
Case 4	0.8	13.7	0.484

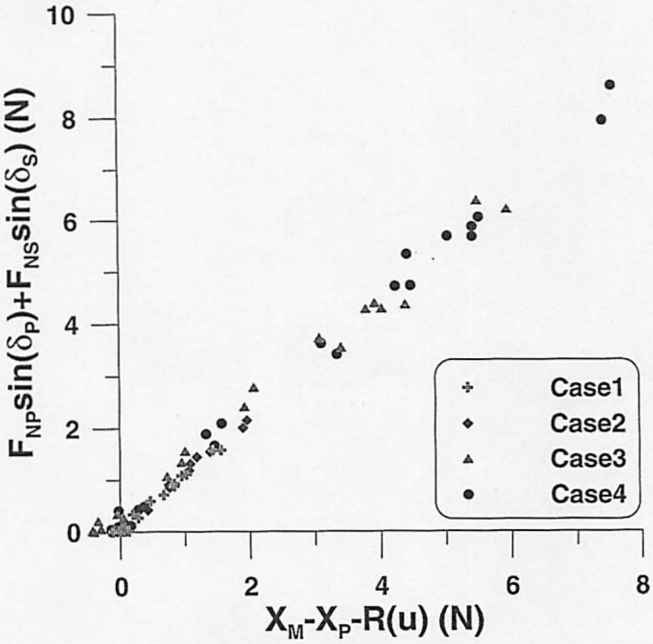

Fig. 14. Interaction between the hull, propeller, and rudder in the surge direction. The cases are explained in Table 5

Fig. 15. Interaction coefficient a_H

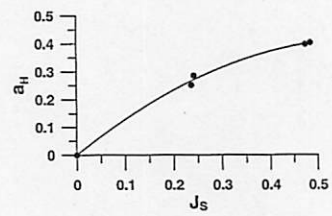

Fig. 16. Interaction coefficient x'_H

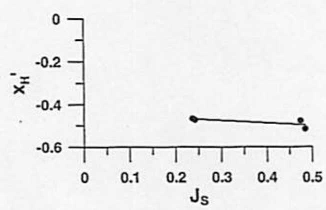

$$
\left.\begin{aligned}
&F_{NS}{}' = \frac{F_{NS}}{\frac{1}{2}\rho A_R U_{RS}{}^2} C_{R1}\mathrm{Tan}^{-1}(C_{R2}\alpha_{RS})\\
&F_{NP}{}' = \frac{F_{NP}}{\frac{1}{2}\rho A_R U_{RP}{}^2} C_{R1}\mathrm{Tan}^{-1}(C_{R2}\alpha_{RP})\\
&U_{RS} = \frac{1}{U}\sqrt{u_{RS}{}^2 + v_{RS}{}^2}\\
&U_{RS} = \frac{1}{U}\sqrt{u_{RS}{}^2 + v_{RS}{}^2}\\
&u_{RS} = C_{RS}(\delta_S) \times \frac{\varepsilon u_P}{1-s}\\
&\qquad \times\sqrt{1-2(1-\eta\kappa)s + (1-\eta\kappa(2-\kappa))s^2}\\
&u_{RP} = C_{RP}(\delta_P) \times \frac{\varepsilon u_P}{1-s}\\
&\qquad \times\sqrt{1-2(1-\eta\kappa)s + (1-\eta\kappa(2-\kappa))s^2}\\
&u_P = (1-\omega_P)u\\
&\kappa = kx/\varepsilon\\
&\eta = D_P/h_R\\
&s = 1 - u_P/nP\\
&v_{RP} = -\gamma_R(v + Lr\cdot u)\\
&v_{RS} = -\gamma_R(v + Lr\cdot u)
\end{aligned}\right\} \quad (11)
$$

Figure 17 shows the rudder normal forces measured during the towing tank experiments. $C_{RP}(\delta_P)$ and $C_{RS}(\delta_S)$ in Eq. 11 were calculated from the experimental data and were used in the simulation utilizing interpolation. It is noted that the rudder forces were only measured for the parallel rudder condition with zero lateral speed and yaw rate of the ship. However, it is assumed that $C_{RP}(\delta_P)$ and $C_{RS}(\delta_S)$ in the straight running condition and the turning condition are not significantly different.

In the current work, simulations were carried out to validate the proposed method and regression model, and the experimental results were used for developing the simulation model. The proposed method can also be used with different rudder and propeller models based on the MMG model; this is because the method here follows the concept of the MMG model.

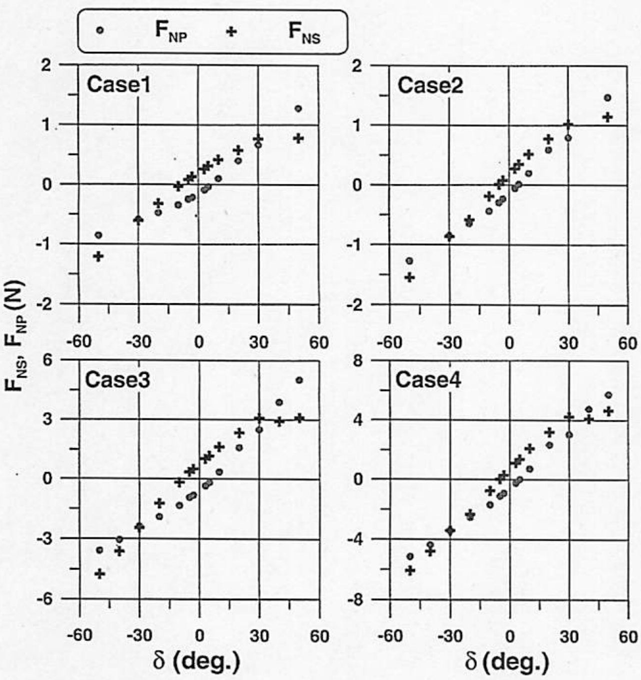

Fig. 17. Measured rudder forces in the parallel rudder condition

Cruising speed simulation

Simulations and free-running experiments for cruising speed were carried out at full speed, which is 0.8 m/s for the model ship and 13.5 knots for the full-scale ship. Figure 18 shows the time histories of the yaw and rudder angles and Fig. 19 shows time histories of the velocity parameters for the –20° zigzag test. The results of the simulation show a small deviation from the experiment at the first overshoot angle, but show good agreement with rest of the experimental data. Figure 20 shows the trajectory of the ship and Fig. 21 shows the time histories of the velocity parameters for a –30° turning test. It may be noted that the turning circle of the simulation is slightly smaller than that of the experiment; however, the time histories of the surge, sway, and yaw rate match well with the experiment results. From the above results, it can be concluded that the proposed method and regression model are suitable for expressing the hull forces of a ship at its cruising speed.

Low-speed simulation

The zigzag test for low speed was carried out at Dead Slow, which is 0.36 m/s for the model ship and 6 knots

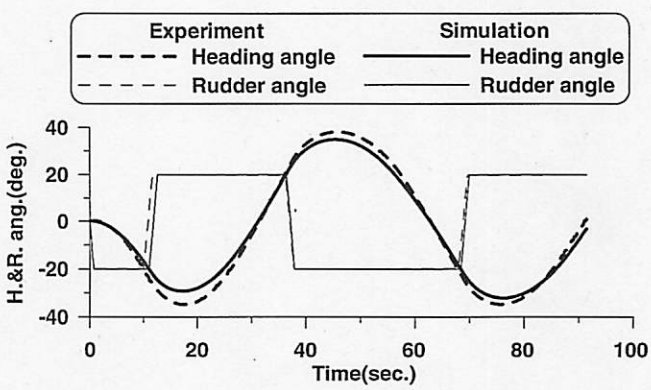

Fig. 18. Heading (H) and rudder (R) angles for the –20° zigzag test at Full Speed

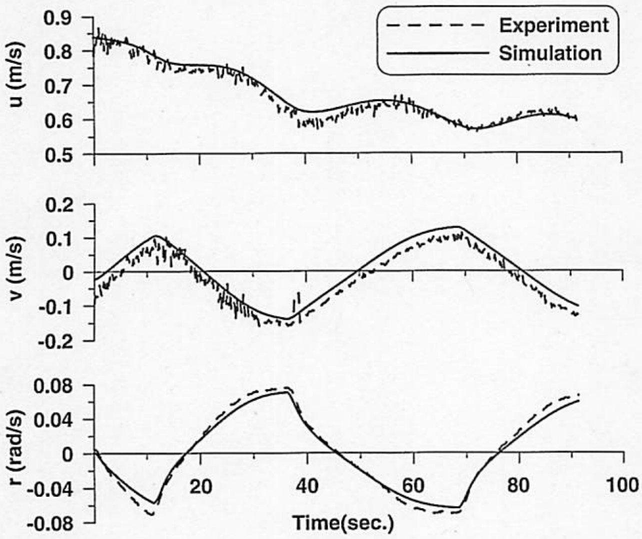

Fig. 19. Velocity parameters for the –20° zigzag test at Full Speed

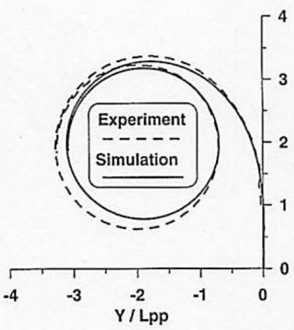

Fig. 20. Ship trajectories for the –30° turning test at Full Speed

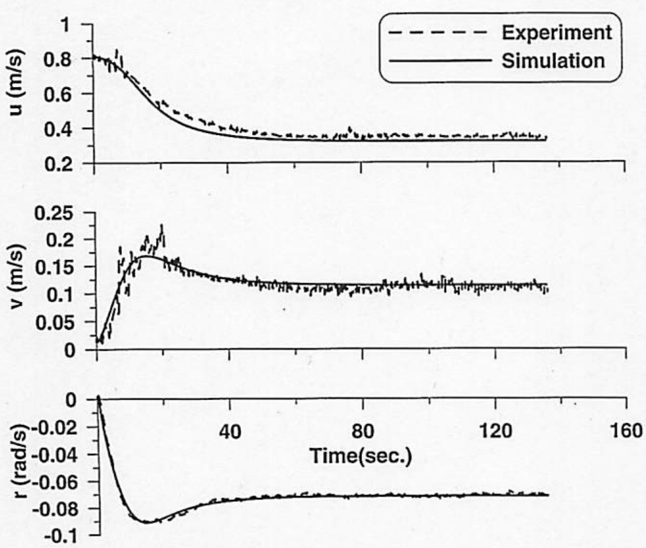

Fig. 21. Velocity parameters for the –30° turning test at Full Speed

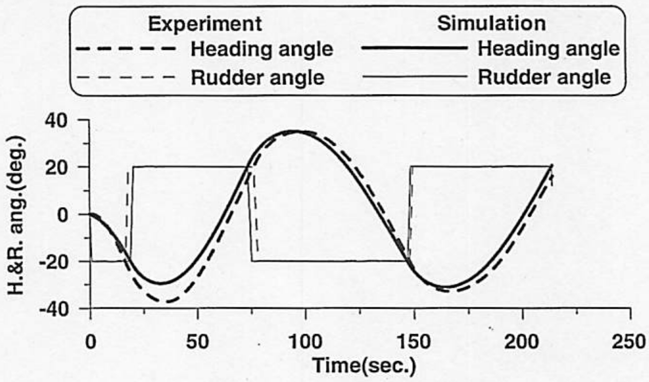

Fig. 22. Heading and rudder angles for the –20° zigzag test at Dead Slow

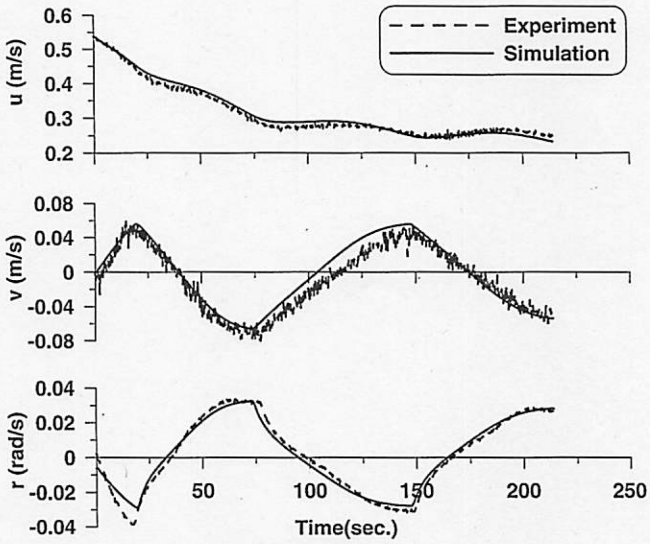

Fig. 23. Velocity parameters for the –20° zigzag test at Dead Slow

for the full-scale ship; however, the initial speed of the experiment was 0.54 m/s. This means that the experiment was started at the commencement of deceleration from Slow to Dead Slow. The initial conditions of the simulation were set as per the above observation. Figures 22 and 23 show the time histories of the parameters during the slow zigzag test. Although the simulation deviates slightly from the experiment during the first overshoot angle, generally, the simulation matches well the experimental data.

Figure 24 shows the trajectory of a ship that starts turning at zero speed. This type of movement can often be observed during a ship's departure from harbor. The propeller revolutions for this experiment and simulation were set to 11 rps, which corresponds to a model ship speed of about 0.6 m/s. Figure 25 shows the time histo-

(1) A practical method for predicting hull forces is proposed. The ability to predict hull forces for maneuvers carried out from low speed to cruising speed was validated with experimental data for the *Esso Osaka*.
(2) A regression model for predicting the hydrodynamic coefficients for the current method is also proposed based on analysis of 21 different blunt-body ships at even keel.
(3) Simulations with the proposed method and regression model were carried out and the results compared with the free-running experimental data at various speeds. The results of the simulations show reasonable agreement with the experimental data.

References

1. IMO MSC 76/23 (2002) Resolution MSC.137(76), standards for ship maneuverability. Report of the maritime safety committee on its seventy-sixth session-annex 6. IMO, London
2. Kijima K, Nakiri Y (2002) On the practical prediction method for ship manoeuvring characteristics (in Japanese). Trans West Jpn Soc Nav Archit 105:21–31
3. Lee TI, Ahn KS, Lee HS, et al (2003) On an empirical prediction of hydrodynamic coefficients for modern ship hulls. In: Proceedings of international conference on marine simulation and ship maneuverability (MARSIM'03), Kanazawa, Japan. RC-1-1–RC-1-8
4. MMG (1980) MMG report V (in Japanese). Bull Soc Nav Archit Jpn 616:565–576
5. Hwang WY, Jakobsen BK, Barr RA, et al (2003) An exploratory study to characterize ship maneuvering performance at slow speed. In: Proceedings of MARSIM'03. RC-16-1–RC-16-14
6. MSS (1989) MSS report IV (in Japanese). Bull Soc Nav Archit Jpn 721:403–411
7. Kobayashi E, Asai S (1984) A study on a mathematical model for maneuvering motions at low speed (in Japanese). J Kansai Soc Nav Archit 193:27–37
8. Yumuro A (1988) Some experiments on maneuvering hydrodynamic forces at low speeds (in Japanese). J Kansai Soc Nav Archit 209:91–101
9. Karasuno K, Okano S, Miyoshi J, et al (2003) Predictions of ship hull hydrodynamic forces and maneuvering motions at slow speed based on a component-type mathematical model. In: Proceedings of MARSIM'03. RC-4-1–RC-4-11
10. Endo M, Hasegawa K (2003) Passage planning system for small inland vessels based on standard paradigms and the maneuvers of experts. In: Proceedings of MARSIM'03. RB-19-1–RB-19-9
11. Hasegawa K (1980) On a performance criterion of autopilot navigation. J Kansai Soc Nav Archit 178:93–104
12. Koyama T, Chyu JH, Motora S, et al (1975) On the circular motion test technique for the maneuverability model test (in Japanese). J Soc Nav Archit Jpn 138:151–157
13. Shoji K, Ramachandran R, Kurobe Y, et al (2002) PMM tests in a circulating water channel and nonlinear analysis. J Mar Sci Technol 7:86–90
14. Mori M (1995) Ship design note ⟨24⟩ (in Japanese). Fune no kagaku 48(3):40–49
15. Hasegawa K, Kang DH, Sano M, et al (2006) Study on maneuverability of a large vessel installed with a mariner type super VecTwin rudder. J Mar Sci Technol 11:88–99
16. Hamamoto M, Enomoto T (1997) Maneuvering performance of a ship with VecTwin rudder system. J Soc Nav Archit Jpn 181:197–204
17. Fujiwara T, Ueno M, Nimura T (1998) Estimation of wind forces and moments acting on ships (in Japanese). J Soc Nav Archit Jpn 183:77–90

Fig. 24. Ship trajectories for the 30° turning test starting from zero speed

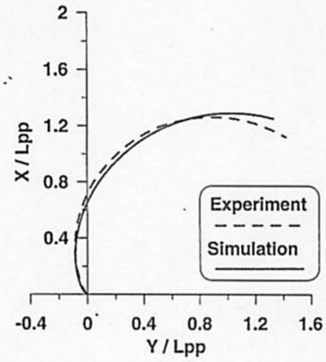

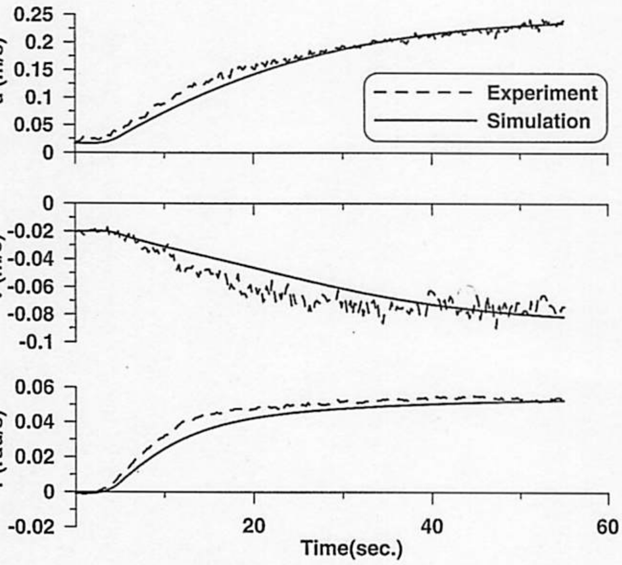

Fig. 25. Velocity parameters for the 30° turning test starting from zero speed

Fig. 26. Ship trajectories for the 20° turning test at Dead Slow

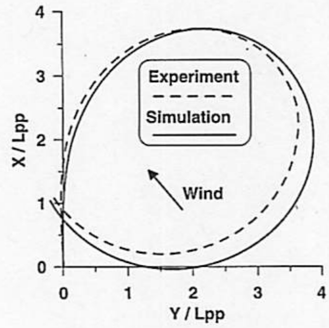

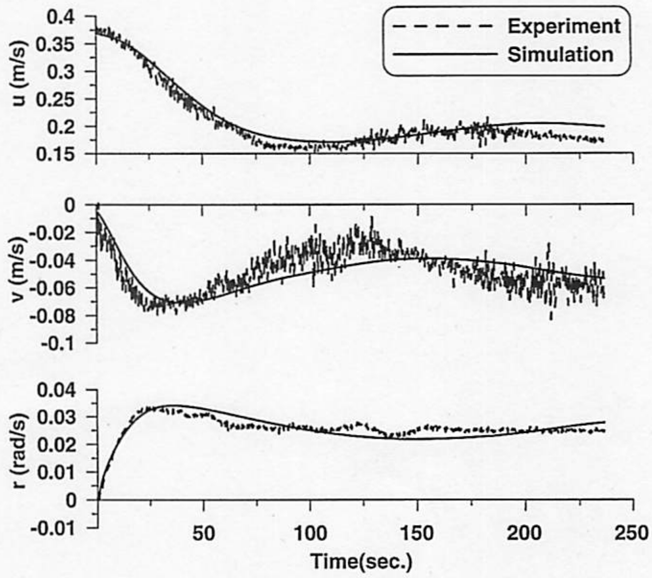

Fig. 27. Velocity parameters for the 20° turning test at Dead Slow

ries of the velocity parameters. From the above results, it can be concluded that the proposed method and regression model are suitable for expressing the hull forces of a ship at low speeds.

Simulation in wind

A ship maneuvering at low speed is easily affected by wind. Prediction of a ship's motion in windy condition is important from the point of view of safety, especially at low speeds. Figure 26 shows a 20° turning test started at Dead Slow in windy conditions. It can be observed from the time histories of the velocity parameters in Fig. 27 that the ship was influenced by wind. Unfortunately, the wind conditions were not measured during the experiment. The wind condition was predicted from the time histories of the velocity parameters and used as a constant wind during the simulation. The predicted wind condition was a wind angle of 140° at 1.7 m/s. Fujiwara's equation[17] was used for calculating wind forces during the simulation. Even though a constant wind condition was used during the simulation, the simulated values matched well the experiment results. From the above results, it can be concluded that the proposed method and regression model are suitable for expressing the hull forces of a ship at low speed even under windy conditions.

Conclusions

This work proposes a practical method of predicting hull forces and also suggests a regression model to predict hydrodynamic coefficients for a blunt-body ship under even keel conditions. The proposed model was validated by comparing the results with experimental data for the *Esso Osaka*. Simulations of a 4-m VLCC ship model with the proposed regression model were carried out and compared with the equivalent free-running experiments to validate the proposed model.